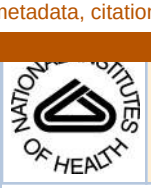

Published in final edited form as:
Biochemistry. 2013 January 29; 52(4): 714±725. doi:10.1021/bi301457f.

Comparative Analysis of Homology Models of the Ah Receptor Ligand Binding Domain: Verification of Structure-Function Predictions by Site-Directed Mutagenesis of a Non-Functional AHR†

Domenico Fraccalvieri[1], **Anatoly A. Soshilov**[2], **Sibel I. Karchner**[3], **Diana G. Franks**[3], **Alessandro Pandini**[4], **Laura Bonati**[1], **Mark E. Hahn**[3], and **Michael S. Denison**[2,*]

[1]Dipartimento di Scienze dell'Ambiente e del Territorio, Università degli Studi di Milano-Bicocca, Milano, Italy

[2]Department of Environmental Toxicology, Meyer Hall, University of California, Davis, California, USA

[3]Biology Department, Woods Hole Oceanographic Institution, Woods Hole, MA, USA

[4]Randall Division of Cell and Molecular Biophysics, King's College London, London, UK

Abstract

The aryl hydrocarbon receptor (AHR) is a ligand-dependent transcription factor that mediates the biological and toxic effects of a wide variety of structurally diverse chemicals, including the toxic environmental contaminant 2,3,7,8-tetrachlorodibenzo-p-dioxin (TCDD). While significant interspecies differences in AHR ligand binding specificity, selectivity and response have been observed, the structural determinants responsible have not been determined and homology models of the AHR ligand-binding domain (LBD) are available for only a few species. Here we describe the development and comparative analysis of homology models of the LBD of sixteen AHRs from twelve mammalian and nonmammalian species and identify the specific residues contained within their ligand binding cavities. The ligand-binding cavity of the fish AHR exhibits differences from mammalian and avian AHRs, suggesting a slightly different TCDD binding mode. Comparison of the internal cavity in the LBD model of zebrafish (zf) AHR2, which binds TCDD with high affinity, to that of zfAHR1a, which does not bind TCDD, revealed that the latter has a dramatically shortened binding cavity due to the side chains of three residues (Tyr296, Thr386, His388) that reduce the internal space available to TCDD. Mutagenesis of two of these residues in zfAhR1a to those present in zfAHR2 (Y296H, T386A) restored the ability of zfAHR1a to bind TCDD and to exhibit TCDD-dependent binding to DNA. These results demonstrate the importance of these two amino acids and highlight the predictive potential of comparative analysis of homology models from diverse species. The availability of these AHR LBD homology models will facilitate in depth comparative studies of AHR ligand binding and ligand-dependent AHR

[2] This research was supported by the National Institute of Environmental Health Sciences (R01ES07685 (MSD), R01ES006272 (MEH) and Superfund Research Grants P42ES004699 (MSD) and P42ES007381 (MEH)) and the California Agricultural Experiment Station (MSD).

[*]To whom correspondence may be addressed: Tel: (530) 752-3879; Fax: (530) 752-3394; msdenison@ucdavis.edu.

Supporting Information

Oligonucleotide sequences used for site-directed mutation of zebrafish AHR1a by PCR (Table S1), sequence alignment and secondary structure attribution of 16 AHRs (Figure S1), ribbon overlay representation of the PASB LBD structure of the sixteen AHRs selected for the comparative analysis (Figure S2), and in vitro expression levels of wild type and mutant zfAHRs, zfARNTs, and mAHR and mARNT (Figure S3). This material is available free of charge via the Internet at http://pubs.acs.org.

activation and provide a novel avenue to examine species specific differences in AHR responsiveness.

Keywords

AH receptor; TCDD; homology model; ligand binding domain

INTRODUCTION

The aryl hydrocarbon receptor (AHR) is a ligand-dependent basic helix-loop-helix (bHLH)/Per-ARNT-Sim (PAS) domain-containing transcription factor that regulates gene expression and other cellular signaling events (1-3). Mechanistically, binding of ligand to the AHR in the cytosol of a cell stimulates translocation of the AHR protein complex into the nucleus and its subsequent dimerization with the ARNT (AHR nuclear translocator) protein transforms the ligand:AHR:ARNT complex into its high-affinity DNA binding form (3-5). Binding of the ligand-activated AHR complex to its specific DNA recognition site, the dioxin responsive element (DRE), stimulates transcription of adjacent genes and thus mediates the toxic and biological effects of AHR ligands (1,3).

Unlike many nuclear receptors, the AHR can bind and be activated by a wide variety of structurally diverse natural and synthetic compounds (6-9), including halogenated aromatic hydrocarbons (HAHs) such 2,3,7,8-tetrachlorodibenzo-p-dioxin (TCDD, dioxin), and the spectrum of biological and toxic effects produced by the ligand-activated AHRs is dependent upon the physicochemical characteristics and metabolic persistence of the ligand (3,7,10). More recent studies have reported that the ligand binding promiscuity of a given AHR may result from differential binding of structurally diverse ligands within the AHR ligand-binding cavity (11-14), similar to the mechanisms responsible for pregnane X receptor ligand binding promiscuity (15,16).

While the lack of any three-dimensional structure information on the AHR ligand binding domain (LBD) has prevented detailed molecular analysis of the mechanisms of AHR ligand binding, we and others have used the availability of crystal and nuclear magnetic resonance (NMR) structures of homologous protein domains to develop homology models of the AHR LBD for such analysis (12,17-20). These theoretical models not only have revealed key structural aspects of the domain, but when coupled with site directed mutagenesis and functional analysis, have proven to be helpful in identifying amino acids important in ligand binding and ligand-dependent AHR activation (12,17-19,21). More recently, these models have been used in molecular docking studies in an attempt to elucidate the detailed interactions of some known ligands (agonists) within the AHR LBD as well as in the virtual screening of collections of putative ligands (12,18-20,22-25). While the binding modes of TCDD and other ligands within the AHR LBD of a given species (typically that of mouse or human AHR) have been predicted by these approaches, experimental confirmation of these proposed interactions are generally lacking. Moreover, until recently, modeling studies have been focused on a limited number of species (12,17-20). The availability of homology models for AHR LBD from a wide variety of species would not only provide avenues to further investigate basic mechanisms of ligand binding and AHR activation, but also to examine mechanisms and structural determinants responsible for the dramatic intra- and inter-species differences that have been observed in AhR ligand binding, ligand selectivity and response (3,10,14,26,27).

Accordingly, here we describe the development and comparative analysis of homology models of the LBD of sixteen AHRs from twelve mammalian and non-mammalian species.

By comparing the volume and shape of the binding cavities in different AHRs, as well as the physicochemical properties of the internal residues, we inferred the role of amino acids that are known to affect TCDD binding affinity. To further assess the value of this approach to predict structure-function relationships, we focused on experimental verification of residues predicted to be important in determining the functional attributes of a fish AhR. Zebrafish (*Danio rerio*) possess three AHRs, one of which (AHR1a) has been shown previously to lack the ability to bind TCDD and DNA and to activate transcription in the presence of TCDD [28,29]. Structural modeling of representative fish AHRs was used to guide site-directed mutagenesis and functional analysis in identifying the specific residues within the zebrafish AHR1a LBD that contribute to its inability to bind TCDD or exhibit TCDD-dependent DNA binding activity. On this basis, zfAHR1a mutants designed to restore TCDD-responsiveness were prepared and experimentally validated, demonstrating the key role of these residues and highlighting the predictive value of the comparative modeling analysis. The proposed approach will not only further contribute to elucidating the mechanisms of AHR ligand binding, but it will provide additional insights into the diversity of AHR ligands and the species-specific differences in AHR responsiveness.

EXPERIMENTAL PROCEDURES

Homology Modeling

The PASB ligand binding domain (LBD) structures of sixteen mammalian, avian and fish AHRs (Table 1) were generated by homology modeling following our previously described protocol (17,18). Briefly, template identification by sequence similarity was performed independently for each target sequence using PSI-BLAST (30) against the Protein Data Bank (31) with default parameters. For all targets, the top hits were the PASB domains of hypoxia-inducible factor 2α (HIF-2α) and ARNT. NMR structures of HIF-2α [PDB ID 1P97 (32)] and ARNT [PDB ID 1X00 (33)] were chosen and the most representative structure in the NMR ensemble of each template was selected using NMRCLUST (34). The two templates were structurally aligned with DALI-Lite (35,36). For each AHR, the target± template sequence alignment was generated with CLUSTALW (37,38) and the result was confirmed using the Align-2D command within MODELLER (39-41). Models of each AHR LBD were built with MODELLER version 8v1 (39-41), a program that implements comparative modeling by satisfying spatial restraints. One hundred candidate models were derived for each target and the optimal model selected was that with the lowest value of the objective function. The quality of the obtained models was assessed by the PROCHECK program (42), which provides information about the stereo-chemical quality, and by the ProSA validation method (43,44), which evaluates model accuracy and statistical significance with a knowledge-based potential. Secondary structures were attributed by DSSPcont (45). This program extends the discrete assignments of secondary structure performed by DSSP (46) to a continuous assignment in the same categories providing increased accuracy. The continuum results are calculated by weighted averages over 10 discrete DSSP assignments with different hydrogen bond thresholds. Three-dimensional visualization and images of the resulting AHR LBD structures were generated using PyMOL (47).

Analysis of Structural Cavities

Identification and characterization of surface pockets and internal cavities in each of the modeled structures were performed with the CASTp server (48). This program allows identification and calculation of the Connolly©s molecular surface and volume for all pockets and cavities in a protein structure. It ranks the cavities by size, where the largest one is usually the binding site. The representations of the resulting cavity surfaces were produced with PyMOL (47).

Chemicals

[^{3}H]TCDD (>99% radiochemical purity) was obtained from Chemsyn Science Laboratories (Lenexa, Kansas, USA) or was a kind gift from Dr. Steve Safe (Texas A&M University). [^{35}S]Methionine was purchased from Amersham (Piscataway, New Jersey, USA) or Perkin Elmer (Waltham, MA) and [^{32}P]γATP was from Perkin Elmer.

Plasmids

The zebrafish AHR1b (zfAHR1b) expression construct pcDNA-zfAHR1b was described previously (29). Expression constructs for zebrafish AHR1a, AHR2, ARNT2b, and ARNT1c (pBKCMV-zfAHR1a, pBKCMV-zfAHR2, pBKCMV-zfARNT2b, and pBKCMV-zfARNT1c, respectively) [28,49-50] were generously provided by Dr. R. Tanguay (Oregon State University, Corvallis, OR, U.S.A.) and Dr. R. E. Peterson (University of Wisconsin, Madison, WI, U.S.A.). In the course of sequencing the pBKCMV-zfAHR1a plasmid, seven single-nucleotide differences in the zfAHR1a cDNA sequence from that of the GenBank zfAHR1a sequence were identified, including two non-synonymous differences resulting in L129I and P280T substitutions in the zfAHR1a protein.

zfAHR1a site-directed mutagenesis, in-vitro protein synthesis and functional analysis

Three amino acid residues (296, 386, and 388) in the ligand-binding domain of zfAHR1a were mutated using the Quick-change XL site-directed mutagenesis kit (Stratagene), following the manufacturers instructions. The pBKCMV-zfAHR1a plasmid was amplified with Pfu polymerase; the complementary primer pairs used for each mutated site are included in the supplemental information (Supplemental Table S1). The primer pair zf1-3868/zf1-c3868 was used to generate a double mutant zfAHR1a at residues 386 and 388. A splicing approach was used to generate the double mutations at positions 296/386 and 296/388, and the triple mutation at 296/386/388. The AgeI/EcoRI fragment containing amino acid residues 350-805 was excised from the Y296H mutant and replaced with the corresponding fragment from each of the other zfAHR1a mutants (386, 388, and 386/388). All mutant zfAHR1a constructs were fully sequenced.

Zebrafish AHR and ARNT proteins were expressed in vitro using the T3-coupled (for pBKCMV constructs) or T7-coupled (for pcDNA3.1 constructs) TNT-Quick Coupled Reticulocyte Lysate Systems (Promega) following the manufacturer©s recommendations. AHR ligand-binding was determined using unlabeled proteins by velocity sedimentation (sucrose gradient centrifugation) analysis in a vertical tube rotor as described previously (51). The TNT reactions were incubated overnight at 4 C with 8 nM [^{3}H]TCDD; nonspecific binding was determined using reactions containing an empty vector (unprogrammed lysate) (51).

For DNA binding analysis, aliquots (1.5 μl) of the indicated in vitro expressed wild-type or mutant AHR and ARNT were combined with 7 μl of MEDG (25 mM MOPS-NaOH pH 7.5, 1 mM EDTA, 1 mM DTT, 10% glycerol) or MEDGK (MEDG supplemented 150 mM KCl) buffer and incubated in the presence of 20 nM TCDD or other compound [or 1% (v/v) DMSO] for 1.5-2 h at room temperature. For zfAHRs, DNA binding analysis was carried out using zfARNT1c because preliminary analyses revealed that it resulted in a greater amount of TCDD-dependent DNA binding than that obtained using zfARNT2b (data not shown). Mouse DRE3-containing oligonucleotide was labeled with [^{32}P]-ATP (Perkin Elmer) and DNA binding (gel retardation) analysis carried out as previously described (52), except that the amount of KCl in the DNA binding incubation was adjusted to a final concentration of 200 mM. DRE bound complexes were separated in native polyacrylamide gels and constitutive and inducible protein-DNA complexes in the dried gel were quantitated using a Fujifilm FLA9000 imager with Multi Gauge software. For protein expression

analysis, zebrafish AHR and ARNT constructs were expressed using TNT system in the presence of [^{35}S]-methionine and aliquots subjected to sodium dodecyl sulfate polyacrylamide gel electrophoresis, followed by fluorography. The amount of radioactivity contained in the bands was either determined by liquid scintillation counting of the excised bands or by imaging analysis using a Fujifilm FLA9000 with Multi Gauge software.

Transient transfection studies in COS-7 cells were carried out to analyze ligand-dependent transcriptional activation by the wild-type and mutant zfAHRs. COS-7 cells were obtained from the American Type Culture Collection (Manassas, VA) and maintained in DMEM (Sigma, St. Louis, MO) supplemented with fetal calf serum (10% final concentration) at 37 C under 5% CO_2. Cells were plated at 5 10 ^{4} cells/well in 48-well plates and transfections were carried out in triplicate wells 24 hours after plating. DNA and Lipofectamine 2000 reagent (Invitrogen, Carlsbad, CA) each were diluted in serum-free DMEM and a total of approximately 300 ng of DNA was complexed with 1 μl of Lipofectamine 2000. The mixture was then added to cells in DMEM with serum. Cells were dosed 5 hours after transfection with either DMSO or TCDD (10 nM final concentration) at 0.5% final DMSO concentration. Renilla luciferase (pGL4.74, Promega, Madison, WI) was used as the transfection control. Transfected DNA amounts were 5 ng each of the AHR expression constructs, 25 ng of ARNT2b, 20 ng of pGudLuc6.1, and 3 ng of pGL4.74. The total amount of transfected DNA was kept constant by addition of pcDNA3.1 vector with no insert. Cells were lysed 18 hours after dosing and luminescence was measured using the Dual Luciferase Assay kit (Promega, Madison, WI) in a TD 20/20 Luminometer (Turner Designs, Sunnyvale, CA). The final luminescence values were expressed as a ratio of the firefly luciferase units to the Renilla luciferase units.

RESULTS AND DISCUSSION

Selection of AHR sequences

Sixteen AHRs (from twelve different species) with known TCDD binding affinity (Kd) data were selected for the generation of the PASB LBD homology models with the goal of comparative analysis of their structural and chemical characteristics and ligand binding cavities. The names, accession numbers and relative TCDD binding affinity classification of the various AHRs used in this analysis are presented in Table 1. Among these AHRs, the C57BL/6 mouse mAHR has been commonly used as the reference AHR for comparison purposes in many studies reporting AHR affinity values from one or several species. The use of a reference AHR in affinity measurements was necessary for these studies since the resulting values usually vary depending on the experimental system, experimental conditions and the ligand binding protocol. Accordingly, TCDD binding affinity estimates for the C57BL/6 mAHR, which is used as the basis for comparisons, are reported to range between 6 pM ± 2.4 nM; this is considered to be high affinity (53-58).

Those AHRs with an affinity for TCDD equal to or greater than that of the C57BL/6 mAHR were classified as having `high' TCDD binding affinity; these included rat, hamster, rabbit, guinea pig, beluga whale, harbor seal and chicken AHRs (Table 1). Those AHRs with TCDD binding affinity that was consistently 3- to 10-fold lower than that of C57BL6 mAHR were designated as having `medium' binding affinity AHRs (Table 1) and included DBA mice and human AHRs (53,55,58,59). The tern AHR also demonstrated an approximately 4- to 6-fold lower TCDD binding affinity than that of high affinity mAHR and chicken AHR, but since [^{3}H]TCDD binding to this AHR was particularly sensitive to washes with detergent-containing buffer (54), it was classified as a `medium/low' affinity AHR (Table 1).

Molecular analysis of several fish species revealed that many contain multiple distinct AHR genes and gene products that vary in their affinity for TCDD (60). For example, killifish contain at least two distinct AHRs, with kfAHR1a having low affinity for TCDD (61) and kfAHR2a having medium TCDD affinity (unpublished results). In contrast, the zebrafish contains three distinct AHRs (zfAHR1a, zfAHR1b and zfAHR2 (28,29,49)). While zfAHR2 has a high affinity for TCDD (Kd ~1 nM), that for zfAHR1b is lower, although it could not be quantitatively determined due to experimental limitations (29). However, based on the approximately 8-fold lower potency of TCDD-dependent activation of transcription in COS-7 cells transiently transfected with zfAHR1b, compared to those containing zfAHR2, zfAHR1b is designated as having a `medium' TCDD-binding affinity (29). Interestingly, in contrast to zfAHR2 and zfAHR1b, zfAHR1a did not demonstrate any detectable [^{3}H]TCDD binding nor transcriptional response to TCDD (28,29).

Homology models and binding cavities

Structural models of the AHR LBDs of the first seven mammalian AHRs in Table 1 were previously obtained by homology modeling (17,18) and structure prediction of the remaining nine sequences was performed as previously described (18). A multiple sequence alignment of the modeled regions (107 residues corresponding to the 278-384 region of mAHR) is presented in Supplemental Figure S1. The HIF-2α and ARNT structures were used as templates because these were the PAS domains with the highest degree of sequence identity with the AHR PAS B (HIF-2α in the range 25-30% and ARNT of about 20%, in the aligned regions) available. For each target sequence, the model with the lowest value of the MODELLER objective function was selected for the subsequent analysis. PROCHECK validation indicated a good stereochemical quality for all the models, with 85 - 94% of residues belonging to the most favored areas of the Ramachandran plot and the overall G-factors ranging from -0.15 to -0.05 (this index ranges from -0.5 to 0.3 for structures solved at 1.5 resolution). Moreover the ProSA z-scores were between -3.29 and -5.25, within the range of values for native protein structures of similar size.

A first comparison of the structural characteristics of the whole set of models indicated that the overall fold was well conserved, as shown in the upper part of Figure 1 by the representative models of mAHR, chAHR and zfAHR2 and, in more detail, in Supplemental Figure S2 by the superimposition of the main-chain of the sixteen models. Small variability is observed only in the loops encompassing a residue insertion (DE loop) and a two-residue deletion (HI loop) of the global alignment with the templates (17). The high structural conservation among the AHR models was also confirmed by the low values of root mean square distance (RMSD) between each model and the reference mAHR model (less than 1 on the Cα atoms). Moreover, the secondary structure attribution was highly consistent, with slight differences only in some connecting loops (see the representative models in Figure 1 and secondary structure attribution for all models in Supplemental Figure S1).

The analysis of structural pockets and cavities, performed by the CASTp server indicates the presence of a buried cavity in the core of each modeled domain. These cavities have internal volumes ranging from 300 - 600 ^{3}, which is within the range (100 - 800 ^{3}) commonly observed in protein binding pockets or cavities (62). Given the somewhat inaccurate assignment of internal side chain conformations associated with the homology modeling procedure, the volume of a given cavity alone cannot be used reliably to predict ligand accessibility. However, the analysis of internal side chains lining the cavity (obtained from the CASTp analysis) can provide insights into their possible steric and physico-chemical interactions with the bound ligand. This analysis helps to understand the role of amino acids at key positions that were previously demonstrated to affect TCDD binding affinity in the mammalian and avian LBDs (53,54,58), as well as to make hypotheses on their role in the fish LBDs.

One avenue to inter-species analysis of LBD properties is comparison of the cavities of the highest affinity receptors in each class. For the mammalian AHRs with relatively high affinity for TCDD (first seven AHRs in Table 1) a ªconsensus cavityº was previously defined as the cavity delimited by the internal residues (obtained by CASTp) that are conserved in all the modeled LBDs (18). This can be viewed as the internal space shared by all these domains, and as such it represents the internal space required for optimal TCDD binding to mammalian AHRs. The cavities of the chAHR and the zfAHR2, both with high affinity for TCDD (Table 1), were taken as reference cavities for avian and fish AHRs. The molecular surfaces that include the selected cavities are shown in Figure 1 (lower panel). The consensus cavity for the high affinity mammalian and the chAHR cavity are very similar in shape and size and, as described below, they also share the same internal conserved residues (see Figure 2A). In contrast, the cavity of the high affinity fish AHR is characterized by a higher number of internal residues (see Figure 3A), associated with a more elongated shape at both sides (delimited by the Fα helix on one side and the C-terminal β-strands on the other). These distinct characteristics suggest a slightly different TCDD binding mode for fish AHRs.

Mammalian and avian AHR LBD models

In high affinity mammalian AHRs, seven internal residues have been shown to constitute the ªTCDD-binding fingerprintº (i.e. the residues identified by site-directed mutagenesis and functional analysis of the mAHR LBD as necessary for optimal TCDD binding (18; Figure 2B and 2C). Of these, Ala375 in the C57BL6 mAHR has been demonstrated to be essential for optimal TCDD binding, since its mutation to valine (17,63) or natural occurrence as valine in the DBA mouse AHR or in the human AHR (V381) (53,58) results in a decreased affinity for TCDD. The position of this amino acid relative to the other fingerprint residues within the internal cavity is illustrated in Figure 2B. When this amino acid is mutated to Val, it introduces steric hindrance at this end of the modeled cavity (Figure 2C), effectively decreasing the cavity volume and potentially affecting ligand interactions with other fingerprint residues (17,18). Thus, a decrease in the internal cavity volume (below that of the consensus cavity) appears to correlate with the decreased TCDD binding affinity observed with AHRs containing other amino acids at position 375 (17,63).

For avian AHRs, the internal residues of the chAHR and tAHR LBD are shown in Figure 2A. Previously, the difference in TCDD binding affinity between the chAHR (high affinity for TCDD) and tAHR (medium/low affinity for TCDD) was attributed to two amino acid substitutions, I324/V325 and S380/A381 (54). Both these substitutions involve residues that are internal to the modeled cavities and that belong to the ªTCDD-binding fingerprintº for mammalian AHRs (18). Since neither of these substitutions significantly changes the shape and size of the internal cavity in the modeled LBD structures (Figure 2D), it is conceivable that TCDD binding in the chAHR LBD may be stabilized by specific interactions with amino acids in or adjacent to these positions. Accordingly, hydrophobic stabilization by the long Ile319 side chain (corresponding to position 324/325 in the ch/tAHR) has been previously suggested to be necessary for optimal TCDD binding by mAHR (18). Therefore, Ile324 in the chicken AHR LBD may stabilize bound TCDD to a higher extent than Val325 present in the tAHR LBD. The role of chicken Ser380 is less clear, since both the high affinity mAHR and the medium/low affinity tAHR have Ala at this position (54). It is possible that optimal electrostatic interactions with the TCDD molecule needed for high affinity binding require the presence of a polar residue, like Ser, in the region defined by the faced residue pair Ser359-Ala375, in mAHR, or Ala364-Ser380 in chAHR. Binding with the tAHR (Ala365-Ala381) lacks this stabilizing effect (Figure 2D). Further studies will be required to understand the underlying mechanism of the A381S-dependent stabilization of TCDD binding to the tAHR. Nevertheless, these modeling results demonstrate that residues

shown to be critical for binding play evolutionarily conserved roles as part of the ligand-binding cavities of AHRs in mammals and birds.

Fish AHR LBD models

The above analyses and previous mutagenesis results (17,18) help to elucidate the importance that the internal cavity size and/or specific amino acid interactions may have in determining TCDD binding affinity. Three zebrafish AHRs have been described (zAHR1a, zfAHR1b and zfAHR2) and while zfAHR2 and zfAHR1b can bind TCDD with high and medium affinity, respectively, zfAHR1a fails to bind TCDD (28,29). As expected, TCDD can stimulate gene expression by zfAHR2 and zfAHR1b, but not by zfAHR1a (28,29). A previous homology modeling study suggested that the inability of zfAHR1a to bind TCDD was due to the presence of different internal cavity residues from those in zfAHR2 that decreased the volume and altered the polarity of the binding pocket itself (20).

Comparison of the internal residues in the zfAHR2 and zfAHR1b modeled cavities (Figures 3A, B, C) indicates that, while most of these residues occupy corresponding positions and are conserved in the two AHRs, a small group lies in different positions. These variations result in differences in the size and shape of the two cavities and, in particular, a slightly reduced space available for the ligand in the zfAHR1b. This steric characteristic is also observed in the modeled cavities of the other two fish AHRs with low or medium TCDD binding affinity, kfAHR1a and kfAHR2a, and it may explain the reduced binding of these AHRs with respect to the zfAHR2.

Comparison of the LBD of the high affinity binding zfAHR2 to that of zfAHR1a, which does not bind TCDD (28,29), revealed a number of different residues, but only four amino acid differences were identified among the internal residues of these LBDs (Figure 3A, D, E). These amino acid differences (H296Y, N341G, A386T and Q388H) result in a dramatically shortened internal cavity in the zfAHR1a model (Figure 3D, E), as a consequence of the high steric hindrance of the side chains of three of the residues in zfAHR1a (Tyr296, Thr386, His388) that causes a break in the internal space available to TCDD, limiting its access to the binding cavity. This was also confirmed by the smaller calculated volume (about 300 ^{3}) and truncated shape of this cavity determined by CASTp in comparison to the internal cavity in zfAHR2 (about 600 ^{3}) which spans the entire domain fold (Figure 3B). Moreover, the presence of different inter-residue interactions in the central part of the cavity may further limit the access of ligand as the Tyr296, Thr386, His388 residues would create a different electrostatic field, and the two facing hydroxyl groups of Tyr296 and Thr386 may generate a network of hydrogen bonds among the side chains.

zfAHR1a LBD mutagenesis and functional analysis

While our analysis and those of Bisson et al. (20) suggest that the steric and electrostatic effects from the side chains of Tyr296, Thr386 and His388 are responsible for the loss of TCDD binding to zfAHR1a, this has not been confirmed experimentally. Accordingly, to test this hypothesis and more generally to evaluate the ability of homology modeling to predict AHR structure-function relationships, individual and multiple mutations (Y296H, T386A and/or H388Q) were introduced into zfAHR1a and the ligand (TCDD) binding and ligand-dependent transformation and DNA binding of the mutant AHRs were determined. These specific amino acid substitutions change the specific zfAHR1a residues into those present in zfAHR2 and, based on our homology model, are expected to increase the internal cavity volume and restore the electrostatic environment of the LBD.

Ligand ([^{3}H]TCDD) specific binding to wild-type and mutant in vitro synthesized zfAHR1a proteins was performed using sucrose density centrifugation. The specific mutations did not affect the level of protein synthesized in vitro from these mutant zfAHR constructs (Supplemental Figure S3). The results of the ligand binding analyses reveal that two of the single mutations, Y296H and T386A, resulted in partial restoration of specific [^{3}H]TCDD binding to the zfAHR1a (Figure 4). Interestingly, [^{3}H]TCDD specific binding to zfAHR1a containing the Y296H+T386A double mutation was not only completely restored, but the amount of binding was 2- to 3-times greater than that observed for the fully functional zfAHR1b or zfAHR2. No increase in [^{3}H]TCDD specific binding was observed with the H388Q mutation and inclusion of this mutation had a negative effect on ligand binding restoration when combined with a T386A mutation, but no effect on AHRs containing the Y296H mutation (Figure 4). While the underlying mechanism of the increased ligand binding of zfAHR1a containing the Y296H+T386A mutation is unclear, it is possible that the enhanced binding may result from increased stability of the AHR LBD and/or AHR protein complex. Given our recent results indicating that one of the binding sites of the AHR chaperone protein hsp90 is contained within the AHR LBD (21), one can envision that increased binding and/or stability of hsp90 within the LBD could further stabilize the AHR, leading to decreased inactivation of AHR ligand binding activity and consequently an increase in the overall amount of [^{3}H]TCDD specific binding. Whether these mutations result in an increase in AHR ligand binding affinity and/or an increase in functional AHRs that can bind ligand remains to be determined. However the stabilizing effects of Y296H and T386A mutations on [^{3}H]TCDD specific binding are consistent with their predicted effect of opening up the ligand binding cavity. Overall, the mutagenesis data confirm the predictions made from comparative analysis of LBD models of the zebrafish AHRs and demonstrate experimentally the importance of amino acids at positions 296 and 386 in facilitating TCDD binding.

The above results demonstrate that insertion of two mutations (Y296H and T386A) can restore ligand binding to the zfAHR1a; however, these analyses do not determine whether these mutations also restore the ability of the zfAHR1a to undergo the ligand-dependent events necessary for AHR transformation and binding to DRE-containing DNA. Accordingly, wild type and mutant zfAHRs were incubated in the absence or presence of 20 nM TCDD and their ability to transform and bind to DNA was determined by gel retardation analysis (Figure 5A). Similar to the ligand binding results described above, TCDD-dependent transformation and DNA binding was observed with zfAHR1a containing the Y296H/T386A double mutation as well as that containing the Y296H/T386A/H338Q triple mutation, with DNA binding by the triple mutant zfAHR1a lower than that of the double mutant. A small but significant increase in TCDD-dependent DNA binding was observed with zfAHR1a containing the Y296H mutation, but not that with T386A or H388Q. Overall, these results suggest that even though partial restoration of ligand binding occurs (~50%) with zfAHR1a containing the Y296H or T386A mutations, the ligand-dependent change in the AHR necessary to stimulate AHR transformation and ARNT dimerization fails to occur. Further studies of these mutations may provide insights into the mechanisms by which ligand binding triggers AHR activation. Interestingly, while the levels of both constitutive and TCDD-inducible DNA binding by zfAHR1b were dramatically higher than those of zfAHR2 or zfAHR1a containing the double mutation, quantitatively, the amounts of the TCDD-dependent enhancement of DNA binding by zfAHR2 and zfAHR1b were similar (Figure 5B). The reason for the increased constitutive DNA binding by the zfAHR1b/zfARNT1c complex is not clear. Interestingly, these DNA binding analysis also revealed for the first time that zfAhR1b:ARNT:DRE complexes can migrate significantly faster in native PAGE gels than complexes formed with AhR2 or the functional AhR1a mutants (Figure 5A). The reasons for these differences in migration remain to be determined. However, it is very likely that the significant differences in the overall size and charge of each of the

zfAhRs (zfAhR2 is 1027 aa with a calculated pI of 7.3, zfAhR1b is 940 aa with a calculated pI of 6.35 and the mut_zfAhR1a is 787 aa with a calculated pI of 8.05), their relatively low amino acid homology (~40%) (28,29), differences in the overall protein conformation/structure of each zfAhR and ultimately their respective zfAhR:ARNT:DRE complexes would be contributing factors. Overall, the site-directed mutagenesis results reveal that the mutations that can fully restore ligand (TCDD) binding activity can also restore TCDD-dependent transformation and DNA binding. These results also demonstrate that the dimerization and DNA binding interfaces of zfAHR1a appear functional and the apparent lack of TCDD-dependent zfAHR1a activation likely results, at least in part, from impaired TCDD binding as a result of selected substitutions within its LBD.

The inability of zfAHR1a to bind TCDD or mediate TCDD-dependent gene expression or toxicity in vivo led to the suggestion that it may be an AHR pseudogene instead of a functional AHR gene (29). Not only does zfAHR1a have an altered LBD that fails to bind TCDD, but previous domain swapping experiments between zfAHR1a and zfAHR2 suggested that the zfAHR1a transactivation domain was also nonfunctional as it failed to confer TCDD-dependent gene expression in transfection experiments when fused to the N-terminal end of zfAHR2 containing functional ligand binding, DNA binding and dimerization domains (28). However, the functional activity of this transactivation domain may be zfAHR1a-specific and may require it to have a functional LBD. Accordingly, to test this, we examined TCDD-dependent transcriptional activity of wild-type and mutant zfAHR1a in COS-7 cells transiently co-transfected with the AhR-responsive luciferase reporter plasmid pGudLuc6.1. While TCDD induced luciferase activity in cells transfected with wild-type zfAHR1b or zfAHR2, no TCDD-induction was observed in cells cotransfected with wild-type or mutant zfAHR1a, irrespective of its ability to bind TCDD or exhibit TCDD-dependent DNA binding (Figure 6). Together, these results extend previous studies demonstrating that the zfAHR1a transactivation domain is nonfunctional, by demonstrating that even changes that dramatically restore ligand binding and DNA binding in a native context (i.e. not a chimeric protein) are insufficient to restore ligand-dependent transactivation function of this AHR.

Given the dramatic structural diversity of AHR ligands, combined with recent evidence of differential binding of such structurally diverse ligands with different residues within the AHR ligand binding cavity (3,11-14), it is possible that while zfAHR1a is unable to bind TCDD-like chemicals, it may still bind and be activated by chemicals that are structurally distinct from TCDD. In fact, molecular docking studies using the AHR LBD homology model identified leflunomide as a possible unique ligand for zfAHR1a (64). In addition, analysis in transgenic zebrafish in which the various zfAHRs had been knocked out or knocked down revealed that leflunomide could induce CYP1A expression in a zfAHR1a-dependent manner (64). These studies suggested that although leflunomide was predicted to bind differently within the LBDs of zfAHR1a and zfAHR2, it was still able to stimulate the same gene induction response and thus must contact common key residues critical for activation of AHR transformation events. Other studies also suggest that zfAHR1a may be functional with certain ligands; Incardona and co-workers have reported that knock-down of zfAHR1a provides protection against the embryotoxicity of pyrene (65). These results not only indicate that the transactivation domain of zfAHR1a is functional, but that its activation appears to occur by a ligand-selective mechanism that is distinct from that of the zfAHR2 transactivation domain. How zfAHR1a is activated by leflunomide and whether other AHR ligands can also bind and activate this AHR remain to be elucidated.

Overall, our findings demonstrate that direct comparison of homology models of AHR LBDs from different species is able to reveal the evolutionary conservation of some key features in the binding cavities of AHRs with high TCDD binding affinity. Moreover, our

experimental results verify the ability of the modeling approach to predict the specific residues that play a critical role in TCDD binding. More generally, the results of this study indicate that comparative analysis of homology models can provide important structural insights into ligand-specific mechanisms of AHR binding and activation that may help to explain some of the dramatic ligand- and species-specific differences in AHR function. Such a mechanistic understanding will inform efforts to explore the AHR as a target for therapeutic intervention and to use the AHR as a molecular biomarker of susceptibility in risk assessment.

Supplementary Material

Refer to Web version on PubMed Central for supplementary material.

Acknowledgments

We thank Dr. Steven Safe (Texas A&M University) for TCDD and [^{3}H]TCDD and Dr. Robert Tanguay (Oregon State University) and Dr. Richard Peterson (University of Wisconsin) for the zebrafish expression vectors. Portions of this work were presented at the 2011 Annual Meeting of the Society of Toxicology (66).

ABBREVIATIONS

AHR	Aryl Hydrocarbon Receptor
mAHR	*Mus Musculus* (mouse) Aryl Hydrocarbon Receptor
zfAHR	*Danio rerio* (zebrafish) Aryl Hydrocarbon Receptor; all other AHR species abbreviations are presented in Table 1
ARNT	Aryl Hydrocarbon Receptor Nuclear Translocator
bHLH	Basic Helix-Loop-Helix
DMSO	Dimethyl Sulfoxide
DMEM	Dulbecco©s Minimal Essential Medium
DRE	Dioxin Responsive Element
HAHs	Halogenated Aromatic Hydrocarbons
HIF-2a	Hypoxia-Inducible Factor 2α
LBD	Ligand Binding Domain
MEDG	25 mM MOPS-NaOH pH 7.5, 1 mM EDTA, 1 mM DTT, 10% glycerol
NMR	Nuclear Magnetic Resonance
PAS	Per-ARNT-Sim
PDB	Protein Data Bank
RMSD	Root Mean Square Distance
TCDD	2,3,7,8-Tetrachlorodibenzo-p-dioxin

REFERENCES

1. Beischlag TV, Morales JL, Hollingshead BD, Perdew GH. The aryl hydrocarbon receptor complex in the control of gene expression. Crit. Rev. Eukary. Gene Express. 2008; 18:207±250.
2. Furness SG, Whelan F. The pleiotropy of dioxin toxicity--xenobiotic misappropriation of the aryl hydrocarbon receptor©s alternative physiological roles. Pharmacol. Ther. 2009; 124:336±353. [PubMed: 19781569]

3. Denison MS, Soshilov AA, He G, DeGroot DE, Zhao B. Exactly the same but different: promiscuity and diversity in the molecular mechanisms of action of the aryl hydrocarbon (dioxin) receptor. Toxicol. Sci. 2011; 124:1±22. [PubMed: 21908767]

4. Soshilov A, Denison MS. Role of the Per/Arnt/Sim domains in ligand-dependent transformation of the aryl hydrocarbon receptor. J. Biol. Chem. 2008; 283:32995±32305. [PubMed: 18806268]

5. Hankinson O. The aryl hydrocarbon receptor complex. Annu. Rev. Pharmacol. Toxicol. 1995; 35:307±340. [PubMed: 7598497]

6. Denison, MS.; Seidel, SD.; Rogers, WJ.; Ziccardi, M.; Winter, GM.; Heath-Pagliuso, S. Natural and synthetic ligands for the Ah receptor.. In: Puga, A.; Wallace, KB., editors. Molecular Biology Approaches to Toxicology. Taylor & Francis; Philadelphia: 1998a. p. 393-410.

7. Safe S. Polychlorinated biphenyls (PCBs), dibenzo-p-dioxins (PCDDs), dibenzofurans (PCDFs), and related compounds: environmental and mechanistic considerations which support the development of toxic equivalency factors (TEFs). Crit. Rev. Toxicol. 1990; 21:51±88. [PubMed: 2124811]

8. Denison MS, Nagy SR. Activation of the aryl hydrocarbon receptor by structurally diverse exogenous and endogenous chemicals. Ann. Rev. Pharmacol. Toxicol. 2003; 43:309±334. [PubMed: 12540743]

9. Nguyen LP, Bradfield CA. The search for endogenous activators of the aryl hydrocarbon receptor. Chem. Res. Toxicol. 2008; 21:102±106. [PubMed: 18076143]

10. Poland A, Knutson JC. 2,3,7,8-Tetrachlorodibenzo-p-dioxin and related halogenated aromatic hydrocarbons: examination of the mechanism of toxicity. Annu. Rev. Pharmacol. Toxicol. 1982; 22:517±542. [PubMed: 6282188]

11. Whelan F, Hao N, Furness SGB, Whitelaw ML, Chapman-Smith A. Amino acid substitutions in the aryl hydrocarbon receptor (AhR) ligand binding domain reveal YH439 as an atypical AhR activator. Mol. Pharmacol. 2010; 77:1037±1046. [PubMed: 20231332]

12. Xing Y, Nukaya M, Satyshur K, Jiang L, Stanevich V, Korkmaz EN, Burdette L, Kennedy G, Cui Q, Bradfield CA. Identification of the Ah-receptor structural determinants for ligand preferences. Toxicol. Sci. 2012; 129:86±97. [PubMed: 22659362]

13. Zhao B, Degroot D, Hayashi A, He G, Denison MS. CH223191 is a ligand-selective antagonist of the Ah (dioxin) receptor. Toxicol. Sci. 2010; 117:393±403. [PubMed: 20634293]

14. DeGroot, D.; He, G.; Fraccalvieri, D.; Bonati, L.; Pandini, A.; Denison, MS. AhR Ligands: Promiscuity in Binding and Diversity in Response.. In: Pohjanvirta, R., editor. The Ah Receptor in Biology and Toxicology. John Wiley & Sons, Inc.; Hoboken, NJ: 2011. p. 63-79.

15. LeCluyse EL. Pregnane X receptor: molecular basis for species differences in CYP3A induction by xenobiotics. Chem. Biol. Interact. 2001; 134:283±289. [PubMed: 11336976]

16. Ngan CH, Beglov D, Rudnitskaya AN, Kozakov D, Waxman DJ, Vajda S. The structural basis of pregnane X receptor binding promiscuity. Biochem. 2009; 48:11572±11578. [PubMed: 19856963]

17. Pandini A, Denison MS, Song Y, Soshilov AA, Bonati L. Structural and functional characterization of the AhR ligand binding domain by homology modeling and mutational analysis. Biochem. 2007; 46:696±708. [PubMed: 17223691]

18. Pandini A, Soshilov AA, Song Y, Zhao J, Bonati L, Denison MS. Detection of the TCDD binding fingerprint within the Ah receptor ligand binding domain by structurally driven mutagenesis and functional analysis. Biochem. 2009; 48:5972±5983. [PubMed: 19456125]

19. Motto I, Bordogna A, Soshilov AA, Denison MS, Bonati L. A new aryl hydrocarbon receptor homology model targeted to improve docking reliability. J. Chem. Inf. Model. 2011; 51:2868± 2881. [PubMed: 21981577]

20. Bisson WH, Koch DC, O©Donnell EF, Khalil SM, Kerkvliet NI, Tanguay RL, Abagyan R, Kollui SK. Modeling of the Aryl hydrocarbon Receptor (AhR) ligand binding domain and its utility in virtual ligand screening to predict new AhR ligands. J. Med. Chem. 2009; 52:5635±5641. [PubMed: 19719119]

21. Soshilov A, Denison MS. Ligand displaces heat shock protein 90 from overlapping binding sites within the aryl hydrocarbon receptor ligand-binding domain. J. Biol. Chem. 2011; 286:35275± 35282. [PubMed: 21856752]

22. O©Donnell EF, Saili KS, Koch DC, Kopparapu PR, Farrer D, Bisson WH, Mathew LK, Sengupta S, Kerkvliet NI, Tanguay RL, Kolluri SK. The anti-inflammatory drug leflunomide is an agonist of the aryl hydrocarbon receptor. PLoS ONE. 2010; 5:e13128. [PubMed: 20957046]
23. Wu B, Zhang Y, Kong J, Zhang X, Cheng S. In silico predication of nuclear hormone receptors for organic pollutants by homology modeling and molecular docking. Toxicol. Lett. 2009; 191:69±73. [PubMed: 19683564]
24. Jogalekar AS, Reiling S, Vaz RJ. Identification of optimum computational protocols for modeling the aryl hydrocarbon receptor (AHR) and its interaction with ligands. Bioorg. Med. Chem. Lett. 2010; 20:6616±6619. [PubMed: 20875740]
25. Murray IA, Flaveny CA, Chiaro CR, Sharma AK, Tanos RS, Schroeder JC, Amin SG, Bisson WH, Kolluri SK, Perdew GH. Suppression of cytokine-mediated complement factor gen expression through selective activation of the Ah receptor with 3',4'-dimethoxy-a-naphthoflavone. Mol. Pharmacol. 2011; 79:508±519. [PubMed: 21127131]
26. Flaveny CA, Murray IA, Chiaro CR, Perdew GH. Ligand selectivity and gene regulation by the human aryl hydrocarbon receptor in transgenic mice. Mol. Pharmacol. 2009; 75:1412±1420. [PubMed: 19299563]
27. Aarts JMMJG, Denison MS, Cox MA, Schalk MAC, Garrison PM, Tullis K, deHaan LHJ, Brouwer A. Species-specific antagonism of Ah receptor action by 2,2©,5,5©-tetrachloro- and 2,2©, 3,3©,4,4©-hexachlorobiphenyl. Eur. J. Pharmacol. 1995; 293:463±474. [PubMed: 8748700]
28. Andreasen EA, Hahn ME, Heideman W, Peterson RE, Tanguay RL. The zebrafish (Danio rerio) aryl hydrocarbon receptor type 1 is a novel vertebrate receptor. Mol. Pharmacol. 2002; 62:234± 249. [PubMed: 12130674]
29. Karchner SI, Franks DG, Hahn ME. AHR1B, a new functional aryl hydrocarbon receptor in zebrafish: tandem arrangement of ahr1b and ahr2 genes. Biochem. J. 2005; 392:153±161. [PubMed: 16042621]
30. Altschul SF, Madden TL, Schaffer AA, Zhang J, Zhang Z, Miller W, Lipman DJ. Gapped BLAST and PSI-BLAST: a new generation of protein database search programs. Nucleic Acids Res. 1997; 25:3389±3402. [PubMed: 9254694]
31. Berman HM, Westbrook J, Feng Z, Gilliland G, Bhat TN, Weissig H, Shindyalov IN, Bourne PE. The Protein Data Bank. Nucleic Acids Res. 2000; 28:235±242. [PubMed: 10592235]
32. Erbel PJ, Card PB, Karakuzu O, Bruick RK, Gardner KH. Structural basis for PAS domain heterodimerization in the basic helix--loop--helix-PAS transcription factor hypoxia-inducible factor. Proc. Natl. Acad. Sci. (U.S.A.). 2003; 100:15504±15509. [PubMed: 14668441]
33. Card PB, Erbel PJ, Gardner KH. Structural basis of ARNT PAS-B dimerization: use of a common beta-sheet interface for hetero- and homodimerization. J. Mol. Biol. 2005; 353:664±677. [PubMed: 16181639]
34. Kelley LA, Gardner SP, Sutcliffe MJ. An automated approach for clustering an ensemble of NMR-derived protein structures into conformationally related subfamilies. Protein Eng. 1996; 9:1063± 1065. [PubMed: 8961360]
35. Holm L, Park J. DaliLite workbench for protein structure comparison. Bioinformatics. 2000; 16:566±567. [PubMed: 10980157]
36. Holm L, Sander C. Protein structure comparison by alignment of distance matrices. J. Mol. Biol. 1993; 233:123±138. [PubMed: 8377180]
37. Thompson JD, Higgins DG, Gibson TJ. CLUSTAL W: improving the sensitivity of progressive multiple sequence alignment through sequence weighting, position-specific gap penalties and weight matrix choice. Nucleic Acids Res. 1994; 22:4673±4680. [PubMed: 7984417]
38. Larkin MA, Blackshields G, Brown NP, Chenna R, McGettigan PA, McWilliam H, Valentin F, Wallace IM, Wilm A, Lopez R, Thompson JD, Gibson TJ, Higgins DG. Clustal W and Clustal X version 2.0. Bioinformatics. 2007; 23:2947±2948. [PubMed: 17846036]
39. Sali A, Blundell TL. Comparative protein modelling by satisfaction of spatial restraints. J. Mol. Biol. 1993; 234:779±815. [PubMed: 8254673]
40. Marti-Renom MA, Stuart AC, Fiser A, Sanchez R, Melo F, Sali A. Comparative protein structure modeling of genes and genomes. Ann. Rev. Biophys. Biomol. Struct. 2000; 29:291±325. [PubMed: 10940251]

41. Fiser A, Do RK, Sali A. Modelling of loops in protein structures. Protein Sci. 2000; 9:1753±1773. [PubMed: 11045621]
42. Laskowski RA, MacArthur MW, Moss DS, Thornton JM. PROCHECK - a program to check the stereochemical quality of protein structures. J. Appl. Crystal. 1993; 26:283±291.
43. Sippl MJ. Recognition of errors in three-dimensional structures of proteins. Proteins. 1993; 17:355±362. [PubMed: 8108378]
44. Wiederstein M, Sippl MJ. ProSA-web: interactive web service for the recognition of errors in three-dimensional structures of proteins. Nucleic Acids Res. 2007; 35:W407±410. [PubMed: 17517781]
45. Andersen CA, Palmer AG, Brunak S, Rost B. Continuum secondary structure captures protein flexibility. Structure. 2002; 10:175±184. [PubMed: 11839303]
46. Kabsch W, Sander C. Dictionary of protein secondary structure: pattern recognition of hydrogen-bonded and geometrical features. Biopolymers. 1983; 22:2577±2637. [PubMed: 6667333]
47. The PyMOL Molecular Graphics System, Version 1.3. LLC; Schr dinger: http://www.pymol.org/
48. Dundas J, Ouyang Z, Tseng J, Binkowski A, Turpaz Y, Liang J. CASTp: computed atlas of surface topography of proteins with structural and topographical mapping of functionally annotated residues. Nucleic Acids Res. 2006; 34:W116±11849. [PubMed: 16844972]
49. Tanguay RL, Abnet CC, Heideman W, Peterson RE. Cloning and characterization of the zebrafish (Danio rerio) aryl hydrocarbon receptor. Biochim. Biophys. Acta. 1999; 1444:35±48. [PubMed: 9931422]
50. Prasch AL, Tanguay RL, Mehta V, Heideman W, Peterson RE. Identification of zebrafish ARNT1 homologs: 2,3,7,8-tetrachlorodibenzo-p-dioxin toxicity in the developing zebrafish requires ARNT1. Mol. Pharmacol. 2006; 69:776±787. [PubMed: 16306231]
51. Karchner SI, Powell WH, Hahn ME. Identification and functional characterization of two highly divergent aryl hydrocarbon receptors (AHR1 and AHR2) in the teleost Fundulus heteroclitus. Evidence for a novel subfamily of ligand-binding basic helix loop helix-Per-ARNT-Sim (bHLH-PAS) factors. J. Biol. Chem. 1999; 274:33814±33824. [PubMed: 10559277]
52. Soshilov A, Denison MS. Role of the Per/Arnt/Sim domains in ligand-dependent transformation of the aryl hydrocarbon receptor. J. Biol. Chem. 2008; 283:32995±33005. [PubMed: 18806268]
53. Ema M, Ohe N, Suzuki M, Mimura J, Sogawa K, Ikawa S, Fujii-Kuriyama Y. Dioxin binding activities of polymorphic forms of mouse and human aryl hydrocarbon receptors. J. Biol. Chem. 1994; 269:27337±27343. [PubMed: 7961644]
54. Karchner SI, Franks DG, Kennedy SW, Hahn ME. The molecular basis for differential dioxin sensitivity in birds: role of the aryl hydrocarbon receptor. Proc. Natl. Acad. Sci. (U.S.A.). 2006; 103:6252±6257. [PubMed: 16606854]
55. Jensen BA, Hahn ME. cDNA cloning and characterization of a high affinity aryl hydrocarbon receptor in a cetacean, the beluga, Delphinapterus leucas. Toxicol. Sci. 2001; 64:41±56. [PubMed: 11606800]
56. Denison MS, Wilkinson CF, Okey AB. Ah receptor for 2,3,7,8-tetrachlorodibenzo-p-dioxin: comparative studies in mammalian and nonmammalian species. Chemosphere. 1986; 15:1665± 1672.
57. Kim EY, Hahn ME. cDNA cloning and characterization of an aryl hydrocarbon receptor from the harbor seal (Phoca vitulina): a biomarker of dioxin susceptibility? Aquat. Toxicol. 2002; 58:57± 73. [PubMed: 12062155]
58. Poland A, Palen D, Glover E. Analysis of the four alleles of the murine aryl hydrocarbon receptor. Mol. Pharmacol. 1994; 46:915±921. [PubMed: 7969080]
59. Denison MS, Hamilton JW, Wilkinson CF. Comparative studies of aryl hydrocarbon hydroxylase and the Ah receptor in nonmammalian species. Comp. Biochem. Physiol. (C). 1985; 80:319±324. [PubMed: 2861016]
60. Hahn ME, Karchner SI, Evans BR, Franks DG, Merson RR, Lapseritis JM. Unexpected diversity of aryl hydrocarbon receptors in non-mammalian vertebrates: insights from comparative genomics. J. Exp. Zool. (A) Comp. Exp. Biol. 2006; 305:693±706. [PubMed: 16902966]

61. Hahn ME, Karchner SI, Franks DG, Merson RR. Aryl hydrocarbon receptor polymorphisms and dioxin resistance in Atlantic killifish (Fundulus heteroclitus). Pharmacogenetics. 2004; 14:131±143. [PubMed: 15077014]

62. Liang J, Edelsbrunner H, Woodward C. Anatomy of protein pockets and cavities: measurement of binding site geometry and implications for ligand design. Protein Sci. 1998; 7:1884±1897. [PubMed: 9761470]

63. Murray IA, Reen RK, Leathery N, Ramadoss P, Bonati L, Gonzalez FJ, Peters JM, Perdew GH. Evidence that ligand binding is a key determinant of Ah receptor-mediated transcriptional activity. Arch. Biochem. Biophys. 2005; 442:59±71. [PubMed: 16137638]

64. Goodale BC, La Du JK, Bisson WH, Janszen DB, Waters KM, Tanguay PL. AHR2 mutant reveals functional diversity of aryl hydrocarbon receptors in zebrafish. PLoS ONE. 2012; 7:e29346. [PubMed: 22242167]

65. Incardona JP, Day HL, Collier TK, Scholz NL. Developmental toxicity of 4-ring polycyclic aromatic hydrocarbons in zebrafish is differentially dependent on AH receptor isoforms and hepatic cytochrome P4501A metabolism. Toxicol. Appl. Pharmacol. 2006; 217:308±321. [PubMed: 17112560]

66. Karchner SI, Franks DG, Pandini A, Soshilov AA, Bonati L, Denison MS, Hahn ME. Testing structure-binding predictions from comparative modeling of the AHR ligand-binding domain: Studies with zebrafish AHR1a. Toxicol. Sci. 2011; 110(The Toxicologist Supplement):79. (Abstract 368).

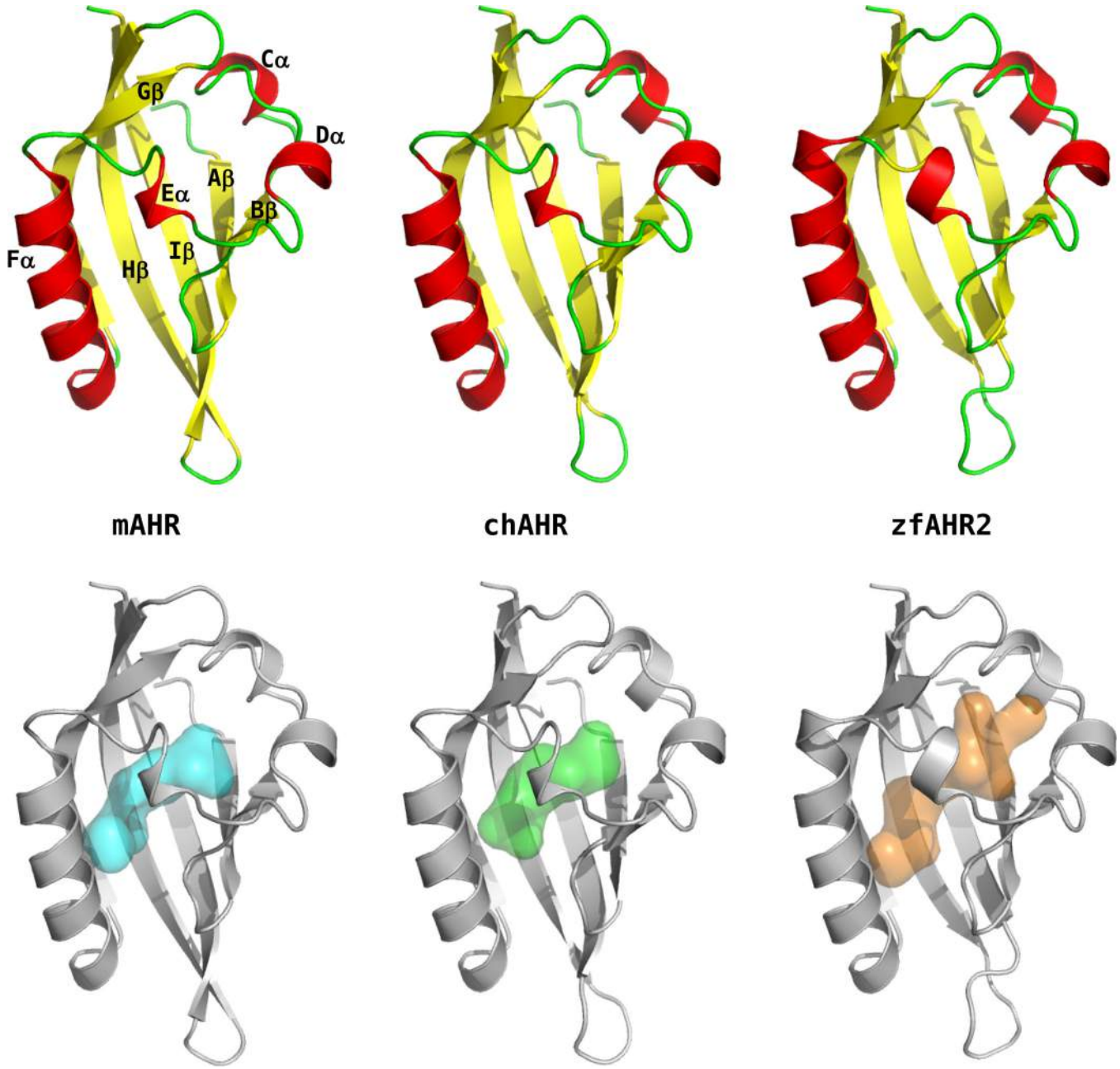

FIGURE 1.

Cartoon representation of the homology models of three AHR LBDs with high affinity for TCDD, representative in each class. In the upper part, mouse, chicken and zebrafish AHR (mAHR, chAHR, zfAHR2) cartoons are colored according to the Secondary Structure attribution obtained by DSSPcont (45) (red: helices, yellow: β-strands). The secondary structure elements of the mAHR are labeled according to the nomenclature generally adopted for the PAS structures. In the lower part, cartoons are colored in grey, and the molecular surfaces that include the consensus cavity of the high affinity mammalian AHRs (cyan), the chAHR (green) and the zfAHR2 (orange) cavities are shown. Representation of the cavity surfaces was produced with PyMOL (47).

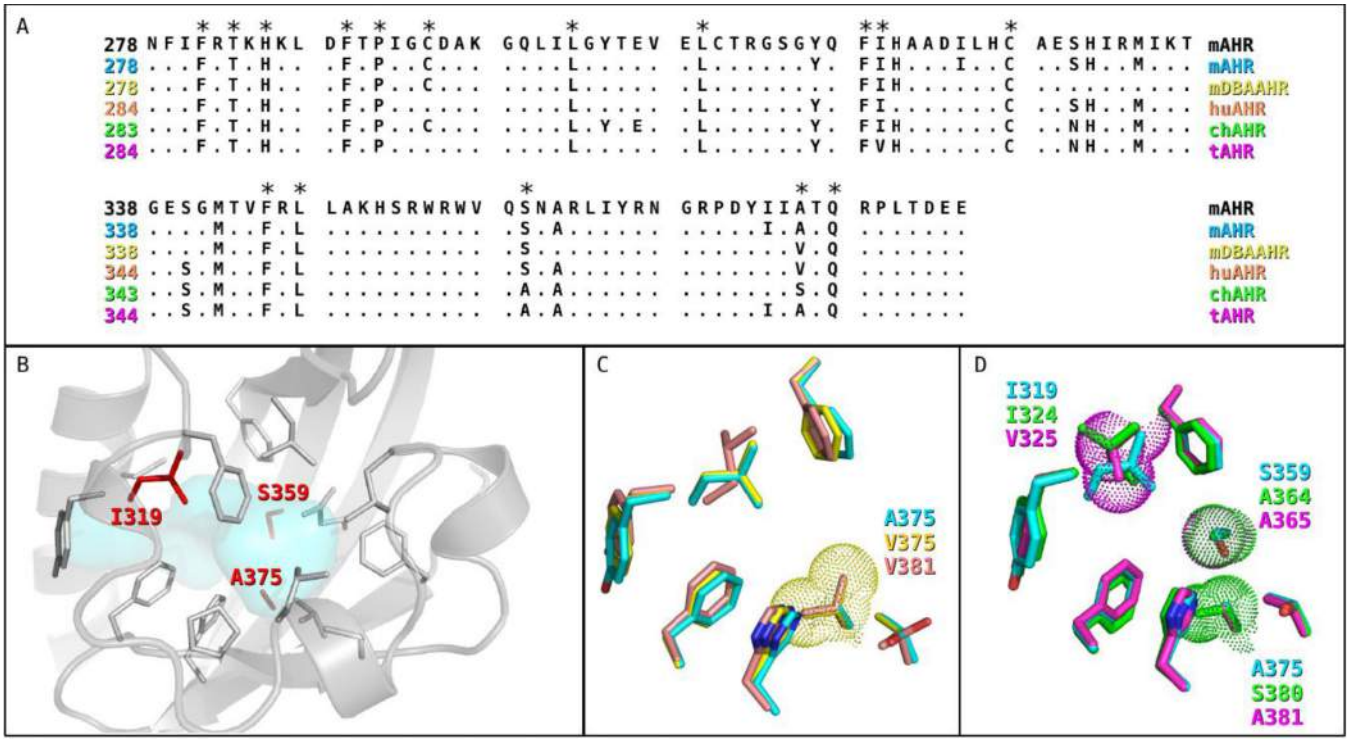

FIGURE 2.

Ligand binding cavities of mammalian and avian AHRs. A. Sequence alignment of selected mammalian and avian AHRs. Except for the mAHR (taken as reference), only the residues identified by the CastP server (48) as internal to the binding cavities are shown. Internal residues conserved in all mammalian AHRs with high affinity for TCDD are indicated by asterisks. B. Cartoon representation of the modeled mAHR LBD. The internal residues conserved in all high affinity mammalian AHRs are shown as grey sticks and the residues that are not conserved in mammalian and avian AHRs with medium or low TCDD affinity are labeled and shown as red sticks. The molecular surface of the consensus cavity for mammalian AHRs is shown in cyan. C. Stick representation of the mAHR (cyan), mDBAAHR (yellow) and huAHR (pink) residues in the ªTCDD binding fingerprintº positions (18). Steric hindrance of unconserved residues is shown as van der Waals spheres around the side chains. D. Stick representation of the residues of the avian AHRs (chAHR in green and tAHR in magenta) in the TCDD binding fingerprint positions, compared to those of mAHR (cyan). Van der Waals spheres are shown around the side chains of unconserved residues.

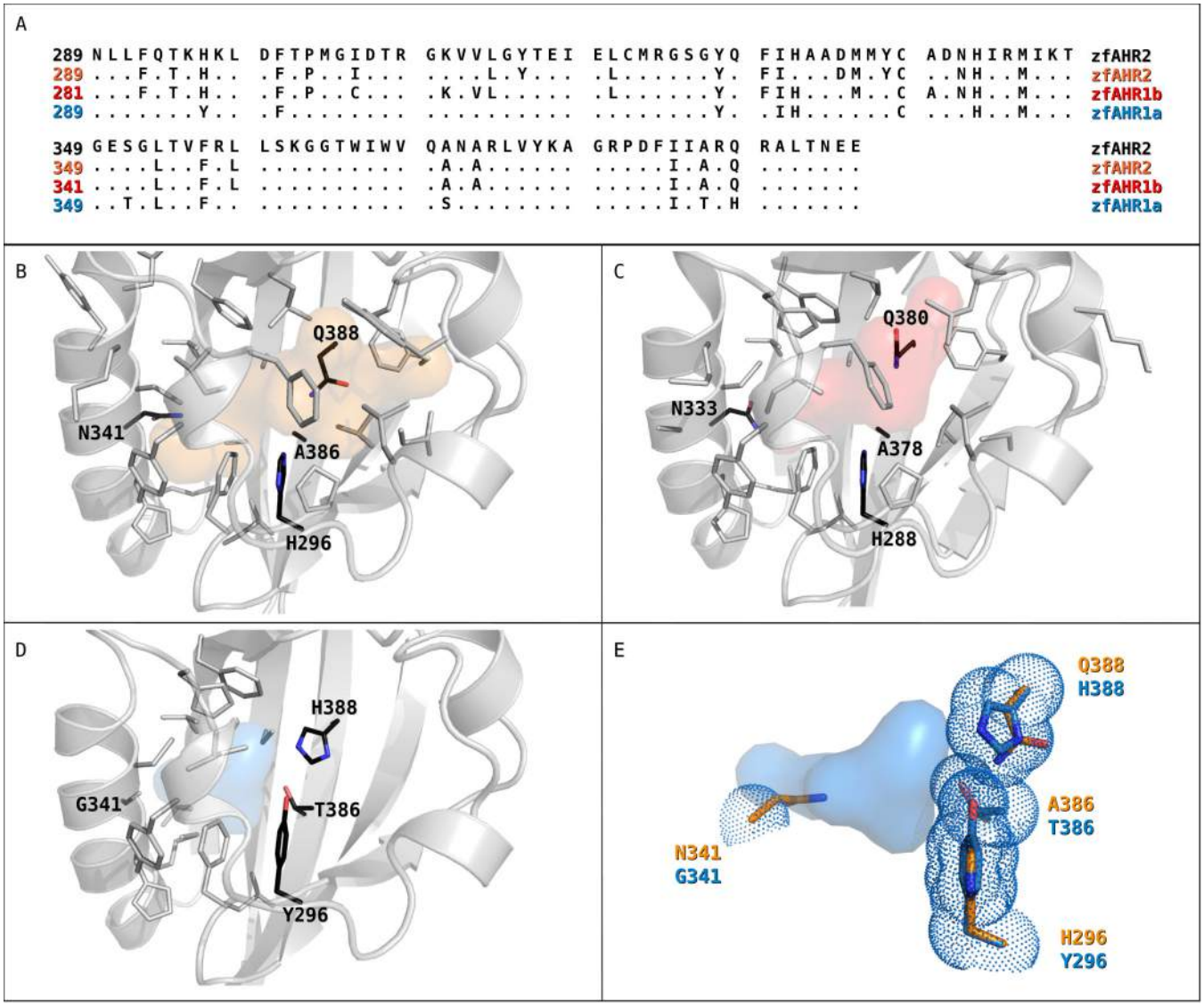

FIGURE 3.

Ligand binding cavities of fish AHRs. A. Sequence alignment of zfAHR2, zfAHR1b and zfAHR1a. Except for the zfAHR2 (taken as reference), only the residues identified by the CastP server (48) as internal to the binding cavities are shown. B. Cartoon representation of the modeled zfAHR2 LBD. The internal residues are shown as grey sticks and the residues that are different in the zfAHR1a (lacks TCDD binding) are labeled and shown as black sticks. The molecular surface of the internal cavity is shown in orange. C. Cartoon representation of the modeled zfAHR1b LBD. The internal residues are shown as grey sticks and the residues that are different in zfAHR1a are labeled and shown as black sticks. The molecular surface of the internal cavity is shown in red. D. Cartoon representation of the modeled zfAHR1a LBD. The internal residues are shown as grey sticks and residues that are different with respect to the zfAHRs that bind TCDD are labeled and shown as black sticks. The molecular surface of the truncated zfAHR1a cavity is shown in blue. E. The steric hindrance of Tyr296, Thr386 and His388 of zfAHR1a (shown as blue Van der Waals spheres) results in truncated internal cavity (blue). The corresponding residues in the high affinity TCDD-binding zfAHR2 are shown in orange.

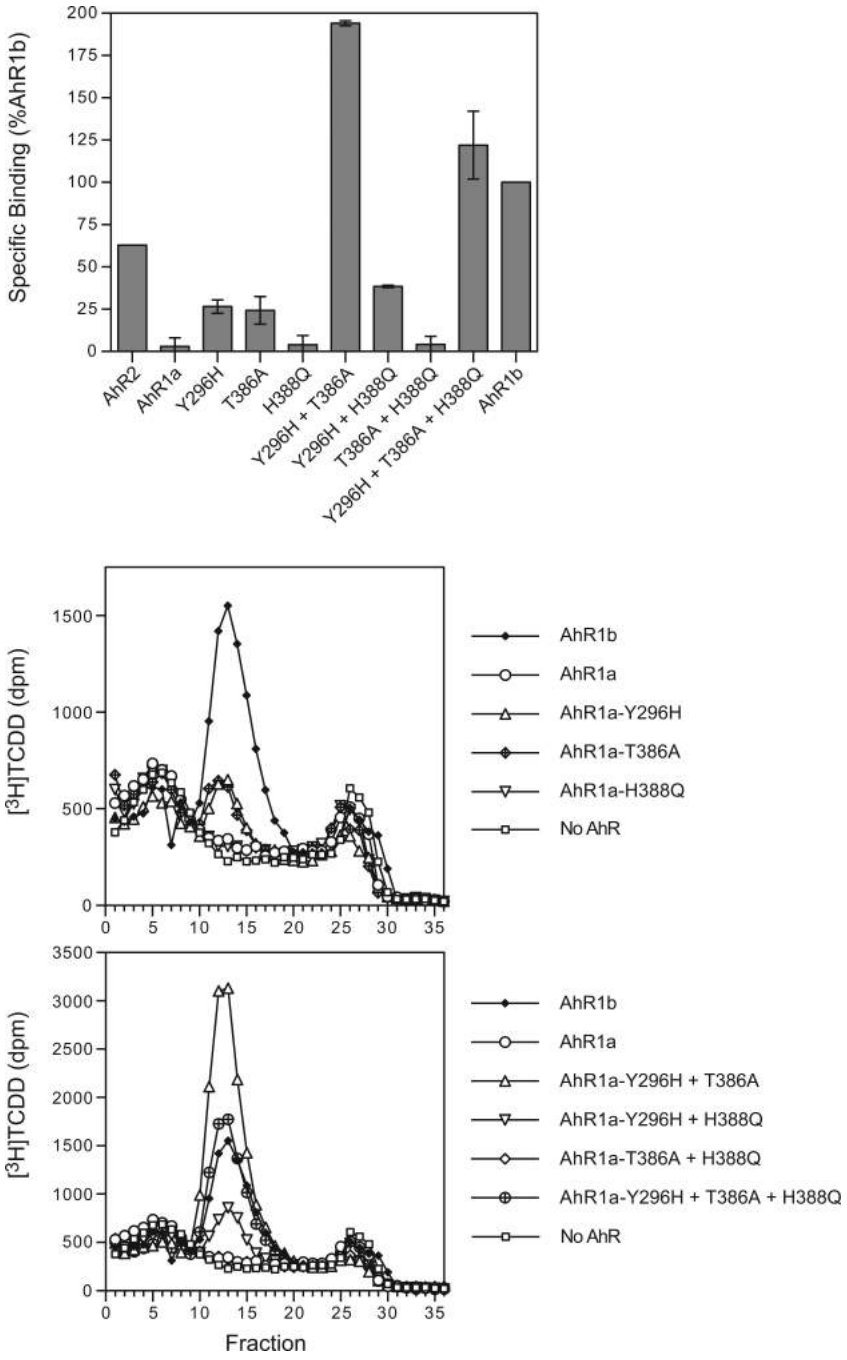

FIGURE 4.

[^{3}H]TCDD specific binding to wild-type zebrafish AHR1a, AHR1b and AHR1a containing various mutations. Wild-type and mutant zfAHRs were synthesized in vitro and subjected to [^{3}H]TCDD ligand binding analysis by sucrose density centrifugation as described under Methods. Specific binding is expressed as a percentage of the specific binding to AHR1b, measured in the same experiment. Top panel shows results compiled from three experiments, with 2 or 3 replicate samples analyzed for each AHR. Bottom panels show representative results from one of the experiments in which all AHRs were analyzed. Note the difference in scale on the two panels.

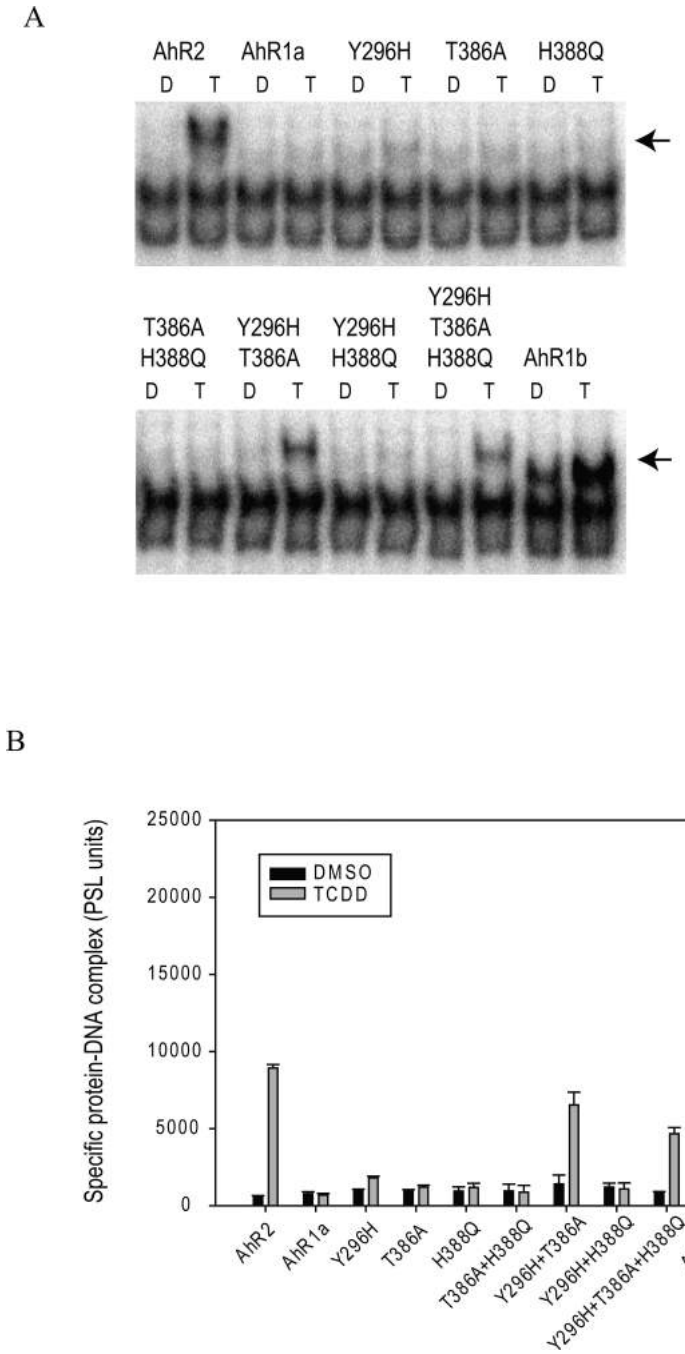

FIGURE 5.

Effect of site-directed mutagenesis of AHR1a on its ability to transform and bind to DNA in a TCDD-inducible manner. A. Wild-type zfAHR2, zfAHR1b, and zfAHR1a containing various mutations were synthesized in vitro, incubated in the presence of DMSO (D) or 20 nM TCDD (T) and transformation and DNA binding assessed by gel retardation analysis as described under Methods. B. Constitutive and inducible protein-DNA complexes in the dried gel were quantitated using a Fujifilm FLA9000 imager with Multi Gauge software and values represent the mean SD of triplicate binding reactions. A typical gel retardation analysis is shown.

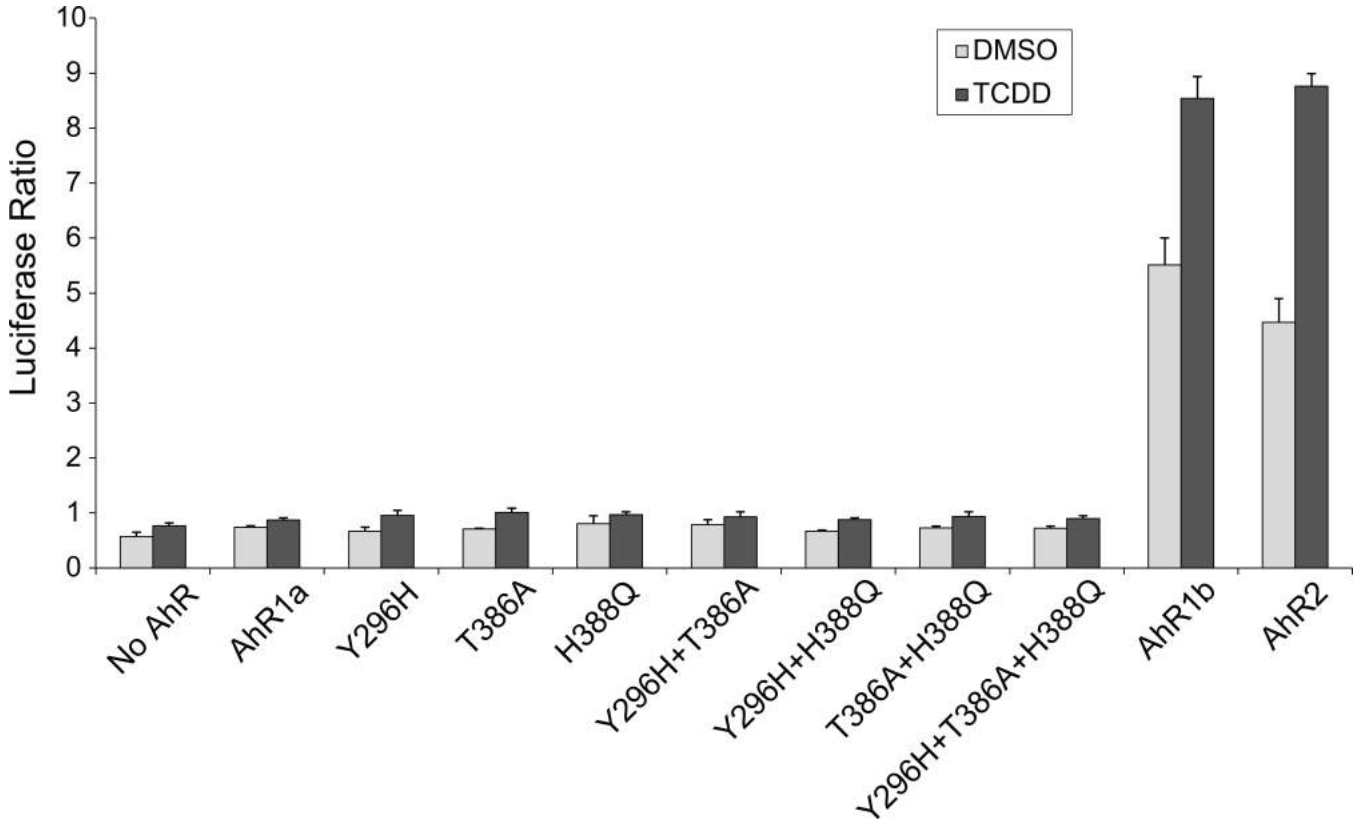

FIGURE 6.

Effect of site-directed mutagenesis of AHR1a on its ability to activate transcription. COS-7 cells were transfected with expression constructs for the zebrafish ARNT2b (25 ng), pGudLuc6.1 (20 ng), pGL4.74 (transfection control), and the indicated AHR expression constructs (5 ng). ªNo AHRº indicates transfection with only the reporter construct and the transfection control. The cells were exposed to dimethyl sulfoxide or TCDD (10 nM). The luciferase activity was measured in a luminometer and the relative luciferase units were calculated by normalizing the firefly luciferase activity to the transfection control *Renilla* luciferase.

Biochemistry. Author manuscript; available in PMC 2014 January 29.

Table 1

AHR sequences selected for the comparative analysis.

	Species	Form	Label	NCBI Acc.	TCDD affinity	Reference
Mammals	Mouse C57BL/6 (Mus musculus)	AHR1	mAHR	NP_038492	High	53,56
	Rat (Rattus norvegicus)	AHR1	rtAHR	AAA56897	High	56
	Hamster (Mesocricetus auratus)	AHR1	haAHR	AAF87578	High	56
	Rabbit (Oryctolagus cuniculus)	AHR1	rbAHR	O02747	High	56
	Guinea Pig (Cavia porcellus)	AHR1	gpAHR	AAT35817	High	56
	Beluga whale (Delphinapterus leucas)	AHR1	bAHR	AAL04031	High	55
	Harbor Seal (Phoca vitulina)	AHR1	sAHR	BAB64569	High	57
	Mouse DBA/2J (Mus sp.)	AHR1	mDBA AHR	AAB32339	Medium	58
	Human (Homo sapiens)	AHR1	huAHR	NP_001612	Medium	53
Birds	Chicken (Gallus gallus)	AHR1	chAHR	NP_989449	High	54
	Common Tern (Sterna hirundo)	AHR1	tAHR	AAF15281	Medium/Low	54
Fishes	Zebrafish (Danio rerio)	AHR2	zfAHR2	NP_571339	High	29
	Zebrafish (Danio rerio)	AHR1b	zfAHR1b	NP_001019987	Medium	29
	Killifish (Fundulus heteroclitus)	AHR1a	kfAHR1a	AAR19366	Low	61
	Killifish (Fundulus heteroclitus)	AHR2a	kfAHR2a	AAC59696	Medium	Hahn unpub.
	Zebrafish (Danio rerio)	AHR1a	zfAHR1a	NP_571103	No binding	28,29, Hahn unpub.